JOURNAL OF GEOPHYSICAL RESEARCH, VOL. 105, NO. A4, PAGES 7403–7417, APRIL 1, 2000

Dynamical effects of geomagnetic storms and substorms in the middle-latitude ionosphere: An observational campaign

Xiaoqing Pi,[1,2] Michael Mendillo,[1] W. Jeffrey Hughes,[1] Michael J. Buonsanto,[3,4] Dwight P. Sipler,[3] John Kelly,[5] Qihou Zhou,[6] Gang Lu,[7] and Terrence J. Hughes[8]

Abstract. An observational campaign was conducted in October 1992 for ~36 hours, at three high- to low-latitude sites near 75°W longitude (Sondre Stromfjord, Millstone Hill, and Arecibo). Vector plasma drift velocities are obtained using the incoherent scatter radar technique at each site. Neutral winds were measured using a Fabry-Perot interferometer, and 6300 Å airglow structures were imaged at the midlatitude site. Electric fields and meridional winds for the period were perturbed when magnetic storms and substorms occurred on the day and night of the campaign. The penetration of magnetospheric electric field and the following interplays between ionospheric electrodynamics and thermospheric wind perturbations in the midlatitude ionosphere are assessed using the multidiagnostic measurements. Evidence for traveling atmospheric disturbances (TADs) and large-scale gravity waves induced by auroral heating effects upon the thermosphere is identified. Diffuse aurora and a stable aurora red (SAR) arc were observed from Millstone Hill during the night of the campaign. The SAR arc moved southward when there were westward electric field perturbations, indicating plasmasphere compression in the postmidnight sector under substorm conditions. The SAR arc location was used to infer the motion of the magnetospheric shielding layer past the Millstone Hill site. Ionospheric F region disturbances in h_mF_2, N_mF_2, and total electron content were driven by the observed dynamics, exhibiting a complex mix of wind and electric field perturbations. While standard model episodes of penetration and shielding/overshielding occurred during the daytime event, such unambiguous clarifications were far less obvious during the nighttime event. This is perhaps due to the prolonged period of moderate geomagnetic activity that served as the background conditions for the substorms that occurred during the campaign.

1. Introduction

Disturbances of the electron density or total electron content (TEC) of the ionosphere (the latter also includes plasmaspheric contribution) are inevitably associated with dynamical processes imposed by energy sources from above (magnetosphere) or below (troposphere-stratosphere). Clear examples of magnetospheric coupling are plasma convection effects, or the electron density irregularities and optical emissions induced by the precipitation of energetic particles. Tides and gravity waves are examples of pure coupling from below. Such a convenient dichotomy is rarely present on a given day. An ever changing blend of sources and perturbation signatures distinguish the hour-to-hour and day-to-day variations of the "real ionosphere" from so-called "first principle models" of the ionosphere. Such models appear fully capable of describing ionospheric variability if the correct blend of time-dependent input parameters can be specified [e.g., *Roble et al.*, 1987; *Schunk and Sojka*, 1989; *Richmond et al.*, 1992; *Pi et al.*, 1993; *Bailey et al.*, 1993; *Fuller-Rowell et al.*, 1994; *Anderson et al.*, 1996; *Sojka et al.*, 1997; *Anderson et al.*, 1998.; *Lu et al.*, 1998; *Richards and Wilkinson*, 1998; *Fuller-Rowell et al.*, 1998].

The observational approach to studies of solar wind induced variability deals, in part, with attempts to specify the thermospheric (neutral wind) and magnetospheric (electrodynamical) drivers of ionospheric dynamics. These tend to dominate the initial phase of a major disturbance (as those associated with a geomagnetic storm), or the full duration of a temporally confined disturbance (as with a magnetospheric substorm). Thermal expansion and neutral composition changes within the thermosphere are fairly well documented and understood and therefore less controversial in the context of current day space physics [e.g., *Prölss*, 1980; *Mendillo et al.*, 1992; *Fuller-Rowell et al.*, 1994; *Burns et al.*, 1995].

[1]Center for Space Physics, Boston University, Boston, Massachusetts.
[2]Now at Jet Propulsion Laboratory, California Institute of Technology, Pasadena.
[3]Atmospheric Sciences Group, Haystack Observatory, Massachusetts Institute of Technology, Massachusetts.
[4]Deceased October 20, 1999.
[5]SRI International, Menlo Park, California.
[6]Arecibo Observatory, Arecibo, Puerto Rico.
[7]High Altitude Observatory, National Center for Atmospheric Research, Boulder, Colorado.
[8]Herzberg Institute of Astrophysics, National Research Council of Canada, Ottawa, Ontario.

Paper number 1999JA900460.
0148-0227/00/1999JA900460$09.00

An excellent review of ionospheric disturbances has recently been given by *Prölss* [1995]. While a proponent of the neutral atmosphere driven sources of F region storm effects, Prölss provides an overview of how electrodynamical processes can also lead to the same types of perturbations. *Buonsanto and Foster* [1993] and *Buonsanto* [1995] have offered some recent observational evidence for the blend of sources during individual events. While these and other studies appear to avoid a firm conclusion on dominant mechanisms, they reflect accurately the current status of the field: it is difficult to capture clear cause-effect relationships in ionospheric disturbances, especially when multiparameter, multisite observations are combined in attempts to reveal a global picture. Particularly important in these studies (and yet still a source of confusion) is the realization that multiple sources (winds and electric fields) do not act in isolation. Winds can generate electric fields, and magnetospherically induced ion drifts can set the thermosphere in motion. Such coupling and feedback processes have different time constants and, given directional constraints imposed by the geomagnetic field, enforcing and/or opposing motions are possible. At middle latitudes it is usually the vertical motions that are the dominant cause of F region electron density changes due to the strong altitude dependence of production and loss mechanisms. Thus vertical motion driven by (1) zonal electric fields, (2) meridional winds, and (3) traveling atmospheric disturbances (TADs) are the key processes to study.

In this paper, we report on a multidiagnostic observational campaign sponsored by the initiative of Coupling, Energetics and Dynamics of Atmospheric Regions (CEDAR) and conducted on October 27-28, 1992; it was one in which considerable effort was made to optimize observing modes for the maximum yield of dynamical effects. The instruments employed were three incoherent scatter radars (ISRs), an all-sky imager, a Fabry-Perot interferometer (FPI), all near 75°W longitude, and a magnetometer chain located in the auroral zone. Such a complement of instruments offers ample capability to record both neutral and electrodynamical effects associated with the disturbances encountered.

2. POSE Campaign

To investigate "Penetration and Overshielding of Substorm Electrodynamics" (POSE), a 2-day campaign was conducted on October 27-28, 1992, using radar and optical techniques. Three ISR facilities in the American longitude sector operated in the modes that are capable of obtaining vector plasma drifts, which can be used to derive both electric fields and meridional winds. The optical instruments were used to observe winds directly and specify emission structures during the nighttime hours.

The Sondre Stromfjord radar (67.0°N, 50.95°W; L=15) collected incoherent scatter data from 0612 UT on October 27 to 1610 UT on October 28, 1992. In each observing cycle (15 min) the backscatter signals were received in nine azimuths at elevation angles of 30°, 55°, and the zenith, followed by an elevation scan in the magnetic meridional plane. The Millstone Hill radar (42.6°N, 71.5°W, L=3.12) operated from 1247 UT on October 27 to 2400 UT October 28, 1992. Throughout the period the Millstone Hill radar observations were conducted with elevation scans in the magnetic meridional plane taking ~22 min to go from *elv* = 9.13° (south) to *elv* = 9.13° (north). The Arecibo radar (18.3°N, 66.75°W, L=1.43) operated between 1427 UT on October 27 and 2223 UT on October 28, 1992. The Arecibo radar observations were conducted at a fixed elevation angle of 75°, with the radar scanning in azimuth through 360° at 26 different angles, first counterclockwise, and then clockwise, taking ~35 min per observational cycle. The drift coefficients, required to compute the vector drift components [*Burnside et al.*, 1987], were obtained for each half cycle and then were averaged to minimize the influence of temporal changes. The Jicamarca radar at the magnetic equator was also scheduled to participate in the POSE campaign but did not operate due to electrical power problems at the time.

During the night of the campaign, at the Millstone Hill site, a Fabry-Perot interferometer was operated by the Atmospheric Sciences Group of the Haystack Observatory, and an all-sky CCD imaging system was operated by the Center for Space Physics of Boston University. To obtain thermospheric winds, the FPI operated in a mode measuring the Doppler shift of 6300 Å atomic oxygen emission in five directions, i.e., northeast, northwest, zenith, southeast, and southwest (with an elevation angle of 30°). Because of the long integration time required to get reasonable quality data, the temporal resolution of wind measurements using this method was ~30 min. Detailed descriptions of the FPI instrumentation and its applications can be found in the work of *Biondi et al.* [1991] and *Sipler et al.* [1991]. Airglow imaging observations were made using filters to capture oxygen emissions at 6300 and 5577 Å about every 3 min, with calibration images at 6444 Å and flat fields, respectively, at the rate of 1 hour per image. Detailed information about an all-sky CCD camera system can be found in the works of *Baumgardner* and *Karandanis* [1984] and *Baumgardner et al.* [1993].

There are chains of magnetometers operating on a daily basis within and around the auroral zone. The magnetic field data from six sites of the CANOPUS magnetometer network [*Rostoker et al.*, 1995] were collected to help identify geomagnetic conditions during the campaign. These six sites cover an area within ~45° in longitude and 7° in invariant latitude, and their locations are shown in Figure 1 together with the coordinates of the three radar sites. Most of the CANOPUS sites are located within the auroral zone (about 65°±5° invariant latitude). For the purpose of comparisons with other measurements, the magnetometer data were smoothed for a time resolution of 1 min.

2.1. ISR Measurements of Electric Fields and Thermospheric Winds

Electric fields can be derived from ISR measurements of the F region vector plasma drift velocity (**V**), assuming the plasma motion perpendicular to the magnetic field ($V_\perp$) is caused by **E**×**B** drift. The vector plasma drift velocities can be obtained through multidirectional measurements of line-of-sight (LOS) ion drift velocities (V_{los}) using a single steerable radar. Owing to the time intervals of the measurements (15, 22, and 35 min for the Sondre Stromfjord, Millstone Hill, and Arecibo radar, respectively), this technique has its limitation and cannot capture rapid changes of electrodynamics that are shorter than the intervals. There are several ways to operate an ISR to obtain relatively slowly changing $V_\perp$ and $V_\parallel$

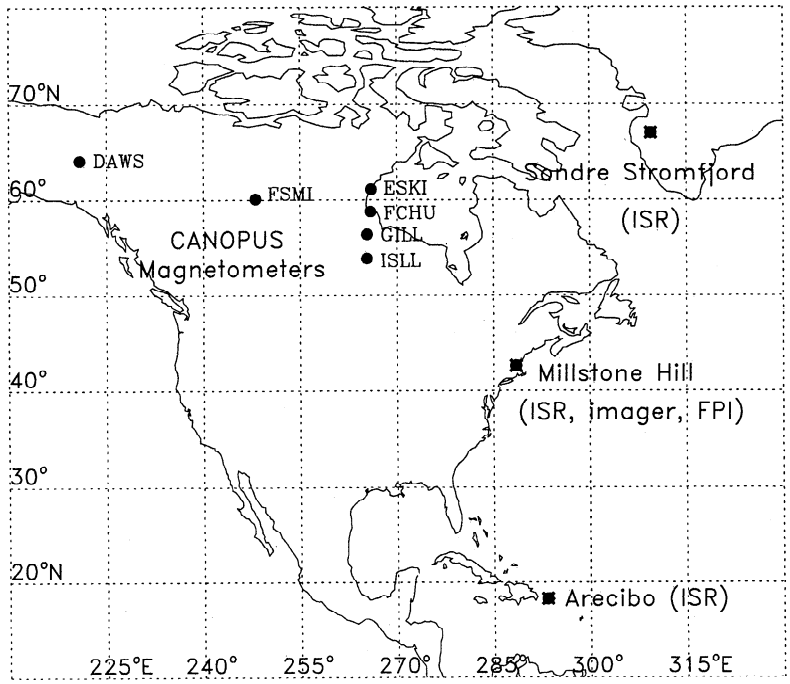

Figure 1. A map showing the coordinates of the POSE observation sites. The instruments included three incoherent scatter radars (ISRs), an all sky imager, a Fabry-Perot interferometer (FPI), and six of the CANOPUS magnetometers.

components. The choice of methods depends on assumptions made to suit experimental circumstances and the degree of precision required [e.g., *Burnside et al.*, 1987; *Buonsanto and Foster*, 1993; *Buonsanto and Holt*, 1995]

Meridional thermospheric winds in the magnetic meridian can be derived from $V_{\parallel}$ and F region plasma diffusion velocities. Calculations of the diffusion velocities need profiles of electron density and temperature, neutral densities ([O], $[O_2]$, $[N_2]$, etc.), and thermospheric temperature. The required plasma parameters can be measured by ISR, while neutral gas parameters can be obtained from an empirical atmospheric model (MSIS86 [*Hedin*, 1987]). The ISR methods of deriving meridional winds can be found in the literature [e.g., *Burnside et al.*, 1983; *Wickwar et al.*, 1984; *Buonsanto et al.*, 1990; *Sipler et al.*, 1991; *Buonsanto and Foster*, 1993], in which the standard diffusion coefficient was applied without additional factors.

3. Results from POSE Campaign

3.1. Magnetic Perturbations

There were moderate geomagnetic storm and major substorm activities during the POSE campaign, as indicated by the geomagnetic indices and magnetometer data shown in Figure 2. In addition to the CANOPUS data, the auroral electrojet *AU* and *AL* indices were also obtained later with magnetic measurements collected from 37 ground stations, which spread in all longitude sectors between 55° and 76° magnetic latitudes. The indices were computed at the National Center for Atmospheric Research using a standard procedure. The substorm activity on October 27 started before the beginning of the experiment and ended at ~1800 UT. This morning activity (LT ~ UT − 6.3 hours in the ~95°W longitude sector) offered a partial opportunity to search for daytime episodes of ionospheric dynamics at middle latitudes associated with substorms. The other major substorm activity occurred during the subsequent nighttime between ~0000 and 1200 UT on October 28. The maximum disturbance amplitude of the magnetic field on the CANOPUS records exceeded 800 nT, occurring at ~1030 UT on October 28. This isolated event thus offered the opportunity to examine the POSE objectives under nighttime conditions. In subsequent figures we will reproduce the third panel of Figure 2 to relate various ionospheric observations to the substorm patterns.

3.2. Electric Fields

The plasma meridional and zonal drift velocities were obtained from the ISR measurements made during the POSE campaign at the Sondre Stromfjord and Arecibo sites, using the methods of 3- and 26-directional measurements, respectively. At Millstone Hill the measurements of V_{los} along zenith and the two adjacent elevations (65.2° north and south) were taken to derive approximately the $V_{\perp N}$ and $V_{\parallel}$ in the magnetic meridional plane, making the usual assumption that gradients of the plasma drifts are small in the region. For the Millstone Hill drift calculations the line-of-sight drift data were averaged over five adjacent points spanning the height range of 300-400 km. The Arecibo data were binned in a height range of 245-405 km, and the drifts were calculated at a mean height of 325 km. At each site, electric fields were derived from F region plasma drifts perpendicular to the magnetic field via $\mathbf{V} = \mathbf{E} \times \mathbf{B}$, where $\mathbf{B}$ values at corresponding altitudes were obtained using the IGRF91 magnetic field model. In all cases, the sign convention will be adopted in which positive values correspond to meridional northward or zonal eastward for electric fields, meridional northward or upward for plasma drifts, and northward for meridional thermospheric winds.

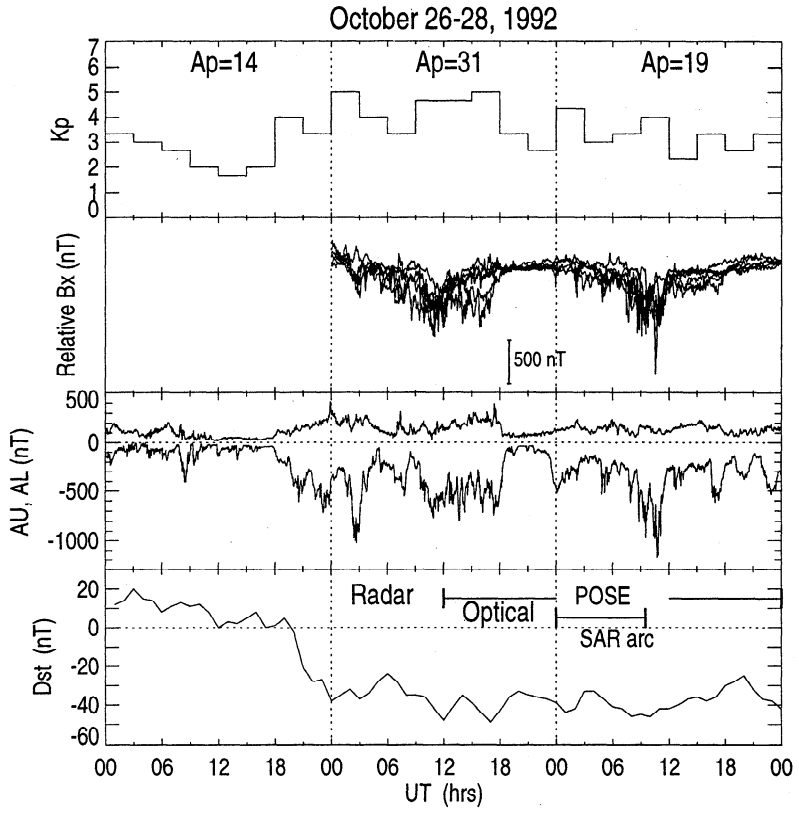

Figure 2. Geomagnetic indices show moderate magnetic storm and substorm activities during October 26-28, 1992. Relative amplitude of the magnetic field B_X component (geodetically northward) of the CANOPUS magnetometer data are plotted in the second panel (from top) to show the features of disturbance. The auroral electrojet *AU* and *AL* indices obtained later is also given in the third panel. The POSE campaign period and the time interval of SAR arc observations are also indicated in the figure.

3.2.1. Meridional electric fields. Figure 3 gives the observational results of meridional electric fields at Sondre Stromfjord and Arecibo; Millstone Hill, operating only in the meridional plane, did not sample zonal drifts. At Sondre Stromfjord, the electric field on October 27 was strongly northward between 1330-1700 UT, and weakly so to 0000 UT, corresponding to the substorm activity and its post recovery. The subsequent appearance of alternately large southward and northward electric field perturbations can be seen during 0000-0600 UT on October 28, a period of rather minor B_x perturbations. During the peak of the substorm on the 28th, the oscillations continued with reduced amplitude. In most cases, the northward bursts upon a generally southward field occur at times of B_x excursions.

In the bottom panel, the Arecibo meridional electric field is compared with its mean pattern obtained from *Fejer* [1993, 1997] for magnetic quiet, equinox, and high solar activity conditions. During the initial substorm event (1200-1800 UT on October 27) the departures from quiet time conditions were slightly northward, but with little evidence for penetration of the strong burst seen at Sondre Stromfjord. On October 28 a sudden transition to large southward electric field appears to follow the Sondre Stromfjord pattern, suggesting penetration at that time. From 0600 to 0900 UT the meridional electric field was southward at Sondre Stromfjord while northward at Arecibo, an overshielding-like effect during a period of increasing B_x activity. At 0900 UT the oscillating northward field is small, with some correlation to the effects seen at Sondre Stromfjord.

3.2.2. Zonal electric fields. The results of the zonal electric fields that drive plasma vertical motions at the three incoherent scatter radar sites are given in Figure 4. At Sondre Stromfjord, eastward perturbations occurred during 1300-1600 UT on October 27, shown in Figure 4b, when enhanced substorm activity can be seen in the CANOPUS magnetometer data (Figure 4a). The zonal electric field at Millstone Hill (Figure 4c) was also disturbed, compared with its quiet-mean drift pattern. It was mainly eastward around noon on October 27 (LT = UT − 4.8 hours) and westward perturbations occurred after 1800 UT which lasted ~5 hours. These orientation changes, alternatively eastward and westward, of the middle latitude electric field seem to be related to the enhancement and subsiding of substorm activity seen in the *AU* and *AL* indices (Figure 4a). The coherence of the eastward fields at both sites may be an indication of the presence of magnetospheric penetration, while the subsequent westward perturbation at Millstone Hill after the substorm decay may be the fossil field or over-shielding effect within the plasmasphere. At Arecibo the zonal electric field, compared also with its mean pattern, was very small during the day of October 27 and essentially in phase with the Millstone Hill results.

On October 28, starting from 0000 UT, the fluctuations of the electric field became stronger at the high-latitude site as the substorm activity began. There were essentially westward fields between 0000 and 0800 UT, perturbed by eastward disturbances near 0300, 0500, and 0630 UT. At the middle and low latitude sites, zonal electric fields were small, with

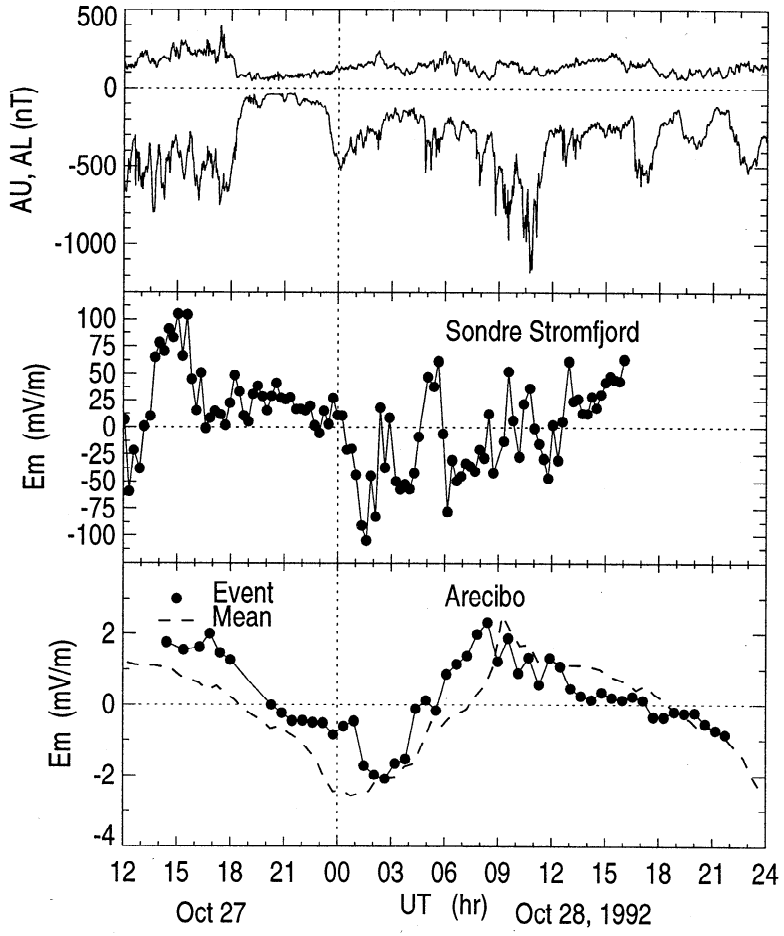

Figure 3. The *AU* and *AL* indices during October 27-28, 1992, are plotted in the top panel. Meridional electric fields (positive northward) derived from the IS measurements of plasma drifts at Sondre Stromfjord and Arecibo, respectively, are given in the middle and bottom panels. A mean pattern under equinox, magnetic quiet, and high solar activity conditions for the meridional electric field at Arecibo is also shown in the bottom panel [*Fejer*, 1993, 1997].

some evidence of these penetration events. As the electrojet enhanced, eastward perturbations of short duration at 0830 and 1030 UT occurred at Sondre Stromfjord and Millstone Hill, but not at Arecibo. Spanning these brief events, the electric fields at Millstone Hill and Arecibo were westward while persistently eastward at the high-latitude site.

Summarizing the electric field patterns in Figure 3 and 4, we find that while the meridional electric field at Arecibo does not show clear correspondence to the high latitude perturbations, the zonal electric fields at Millstone Hill and Arecibo show perturbations associated with substorm activities; the perturbation patterns indicate that zonal electric field penetration processes might have occurred at Millstone Hill during the daytime on October 27 and nighttime on October 28. At Arecibo the dominant zonal electric field perturbation was a westward surge in the postmidnight period on October 28.

3.3. Meridional Neutral Winds

Plasma drifts along the magnetic field line ($V_{\parallel}$) were also obtained using radar techniques to derive thermospheric winds at Millstone Hill and Arecibo. Plasma diffusion velocities (needed for wind determination) at Millstone Hill were calculated at the F region peak where the altitude gradient of electron density is zero. The electron and ion temperatures used for the wind calculations at this site are averaged over five measurements made at adjacent heights (~20 km height intervals) to lessen possible noise in the data. The winds at Arecibo are calculated at the height of 325 km. The required neutral densities and temperatures are obtained via the MSIS86 atmospheric model [*Hedin*, 1987] for the corresponding geophysical conditions. During the nighttime hours, direct Doppler measurements of neutral winds at the Millstone Hill site were obtained using the FPI technique. Thus, in presenting wind patterns, we will describe October 28 first. Unfortunately, FPI observations were not conducted at Arecibo.

The FPI measurements at Millstone Hill show a southward meridional wind during the evening hours (~0000-0500 UT) on October 28, shown in Figure 5b. Meridional winds derived using the ISR method at the same site, shown in Figure 5c, basically match the FPI measurements during the same hours. The wind at Arecibo during the same hours (Figure 5d), derived from the ISR measurements, appears to be oscillating between southward and northward directions, implying possible gravity wave activity which is confirmed through examining electron density data (in a later section). The overall wind pattern during this period shows the usual diurnal behavior of equatorward winds at nighttime; yet they

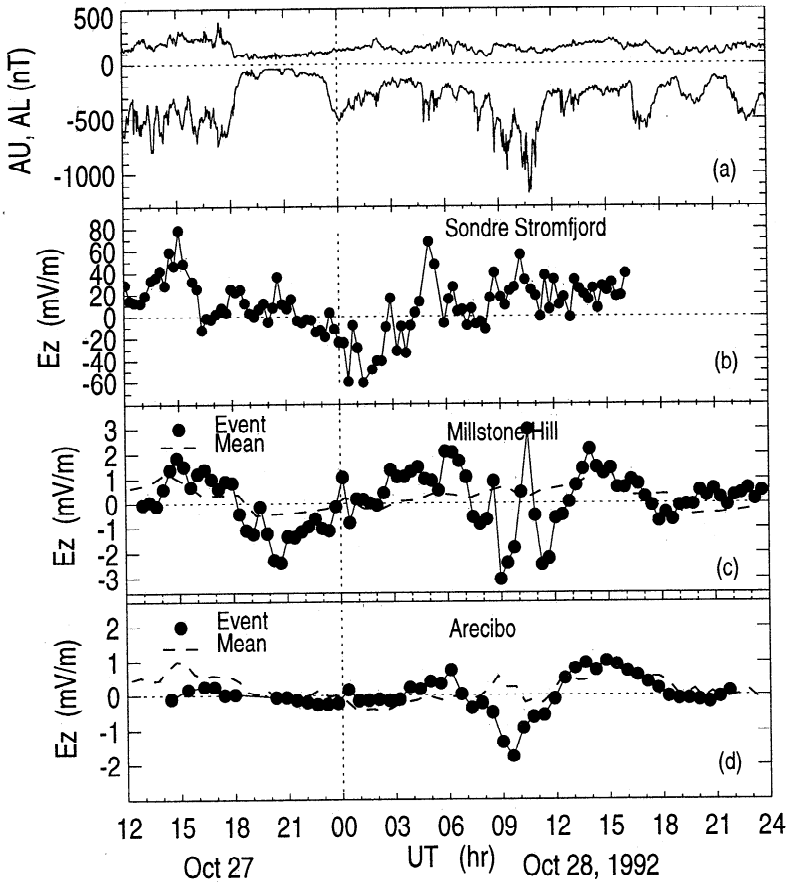

Figure 4. Plotted are the auroral electrojet *AU* and *AL* indices (a) during October 27-28, 1992, and the zonal electric fields (positive eastward) derived from the ISR measurements of plasma drifts at (b) Sondre Stromfjord, (c) Millstone Hill, and (d) Arecibo. The mean patterns for the zonal electric fields under the equinox, magnetic quiet, and high solar activity conditions at the middle-latitude sites are also shown in Figure 4c and 4d, respectively [*Buonsanto et al.*, 1993; *Fejer*, 1993].

appear earlier and have stronger values at Millstone Hill than the pattern given by an empirical wind model (HWM90 [*Hedin et al.*, 1991]) for that site. The maximum equatorward wind occurred about an hour earlier (~0230 UT) at Millstone Hill (versus ~0315 UT at Arecibo), suggesting a TAD event starting near 0000 UT. The subsequent abatement in the southward winds occurs earlier than in the HWM90 model, with larger winds at Arecibo suggesting an earlier occurrence of the "midnight collapse" effect (see next section).

The winds during the daytime periods of both October 27 and 28 show consistent reductions from the model predicted poleward winds. These perturbations are probably associated with Joule heating caused by the substorm activity that occurred prior to 1200 UT (0700–0800 LT) each day. Superimposed upon these overall reductions in northward winds at the two sites are patterns that are perturbed in opposite directions. For instance, the wind at Millstone Hill is northward during 1630-1900 UT on October 27, while southward at Arecibo. The winds at both sites are again out of phase until ~0000 UT on the next day. As shown in Figure 2, the first substorm during POSE occurred during the main phase of a geomagnetic storm. During this period, equatorward wind surges or TADs may arise from both auroral zones, and large-scale gravity waves may propagate from high to low latitudes, providing ample opportunity for phase varying perturbations.

3.4. Ionospheric Disturbances at the Middle Latitudes

The ionospheric electron density effects at Millstone Hill and Arecibo throughout the campaign are shown in N_mF_2, h_mF_2, and TEC in Figure 6 are measured using the IS radars at the two sites. The TEC values are obtained via integration over vertical electron density (N_e) profiles between 140 and 600 km for the Millstone Hill site, and N_e between 100 and 600 km measured from each azimuth (at a fixed elevation of 75°) for the Arecibo site. Plate 1 plots the contour (coded in color) of electron density as functions of universal time and altitude measured at the two sites.

On the day of October 27 a partial diurnal double maxima (DDM) feature appeared in TEC at Arecibo under substorm conditions (Plate 1d). A similar DDM pattern, however, was not seen at Millstone Hill. This indicates that the Arecibo DDM event has a characteristic differing from the one we have discussed before [*Pi et al.*, 1993, 1995], in which DDM occur simultaneously at middle and lower latitudes. The Arecibo DDM event (already in progress when Arecibo started observing at 1500 UT) seems to follow the variations of h_mF_2 that are related to meridional winds (alternatively northward and southward, in Figure 5), rather than to electrodynamics (the eastward electric field is small in Figure 4). The hint of a DDM pattern during the daytime of October 28 (again more in Arecibo TEC and N_mF_2 than at Millstone Hill) coincided with eastward electric field penetration effects

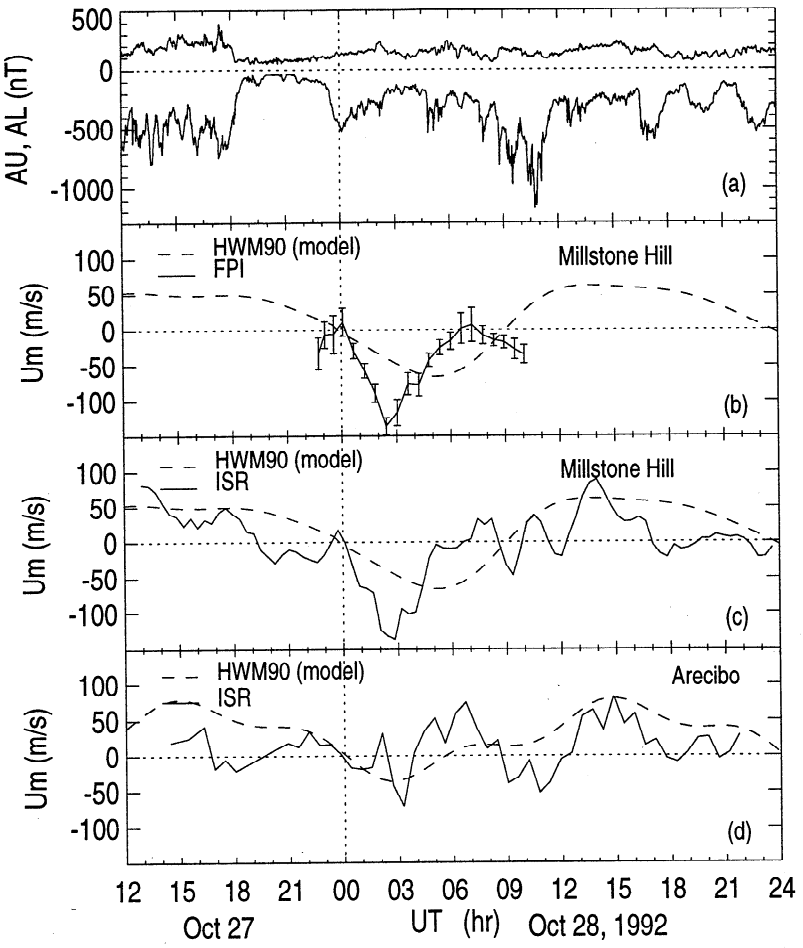

Figure 5. Plotted are thermospheric winds in the geomagnetic meridians during October 27-28, 1992, at Millstone Hill and Arecibo, obtained using the FPI and ISR techniques. In all panels, positive winds are northward. The HWM90 model winds [*Hedin et al.*, 1991] are also plotted in comparison with the measurements. The auroral electrojet *AU* and *AL* indices are shown in Figure 5a to give the context of substorm activity.

at ~1400 UT. For October 27, however, the equatorward wind (1700-1900 UT, Figure 5) at Arecibo responsible for the uplifting may be related to the substorm TAD (or large-scale gravity wave) effects which seem to appear earlier at Millstone Hill and cause a reduction in the northward wind. At Millstone Hill, TEC and N_mF_2 reached the maximum at ~1700 UT when a decrease occurred at Arecibo, and then continuously decreased to lower values following a h_mF_2 decrease between 1800 and 2000 UT. The decrease of h_mF_2 at Millstone Hill seems to be caused by a westward electric field during the corresponding period (Figure 4). The continuous reductions in both TEC and N_mF_2 at later hours at Millstone Hill can be attributed partially to the normal diurnal variation, and partly to a combined effect of a zonal electric field (westward, Figure 4) and a meridional neutral wind (poleward, Figure 5) that cause downward plasma motion. In addition, the neutral composition changes during the recovery phase of a storm (i.e., decreases of the O/N_2 density ratio) may also act to cause the reduction of ionospheric electron density and TEC in the subauroral region.

With the onset of geomagnetic activity at 0000 UT on October 28, some of the more dramatic effects in the *F* region at Millstone Hill and Arecibo occurred. For instance, a wave-like perturbation was observed in h_mF_2 and N_mF_2 as well as TEC at Arecibo after local sunset on October 27. In Plate 1 the wave-like feature can be seen in the N_e variations from the bottomside to the topside ionosphere. Compared with wind data at the same site shown in Figure 5d, this ionospheric wave-like behavior corresponds to alternatively southward and northward wind perturbations. This indicates that a gravity wave is the source of the wave-like ionospheric disturbance. The wave-like disturbance was not seen in the Millstone Hill records. At Millstone Hill a rapid increase of h_mF_2 was observed between 0000 and 0100 UT on October 28, which was caused by the enhanced nighttime equatorward wind shown in both ISR and FPI records (Figure 5b and Figure 5c). At later hours (0400-0800 UT), while the Millstone Hill h_mF_2 kept high (over 350 km), a h_mF_2 decrease ("midnight collapse") of ~100 km caused by a poleward wind (Figure 5d) was observed at Arecibo.

As the magnetic activity increased during 0700-1100 UT on October 28, the Arecibo h_mF_2 (Figure 6c) rapidly rose to 360 km, an increase of ~80 km, and the Millstone Hill h_mF_2 reached the same height. N_mF_2 and TEC as well as N_e in the whole altitude ranges (Plate 1) at both sites gradually decreased until they dropped to the lowest levels before sunrise. The dynamics at the two sites are much more complicated during the period so that only basic patterns are summarized here and more discussions will be given in a later section. On one hand, zonal electric fields at both sites were

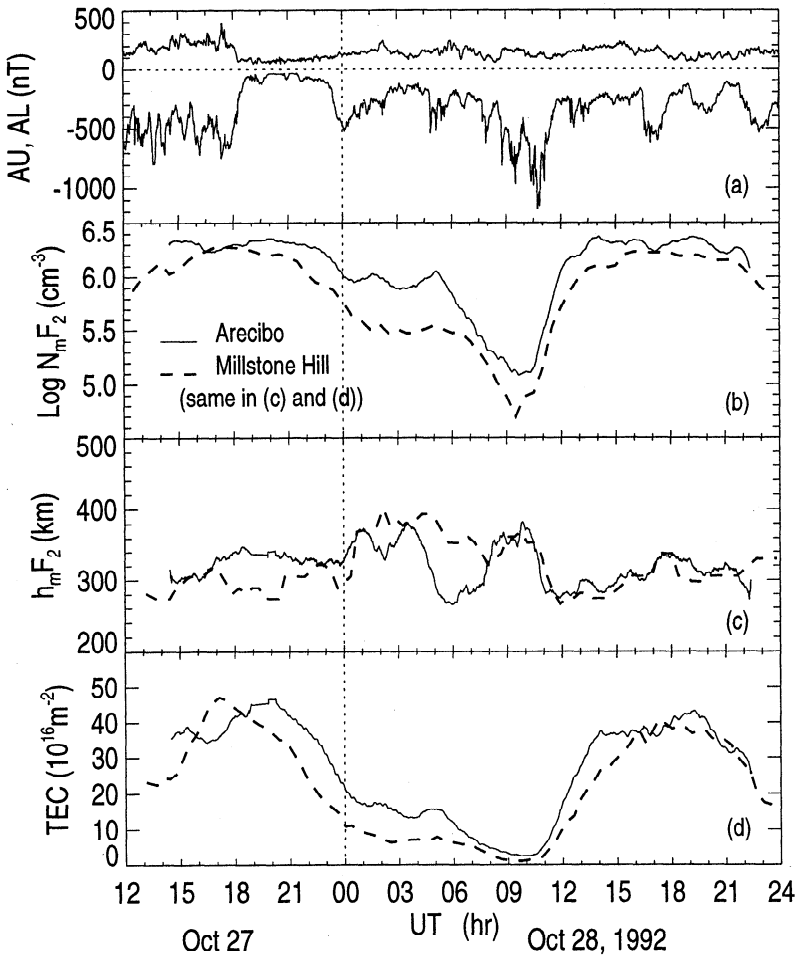

Figure 6. (a) The magnetic *AU* and *AL* indices during October 27-28, 1992; (b) the maximum electron density of the ionospheric F_2 region, (c) heights of the maximum electron density, and (d) TEC integrated from the N_e profiles obtained through incoherent scatter radar measurements at Millstone Hill and Arecibo.

mainly westward (recalling Figure 4d). On the other hand, the meridional wind was southward at Arecibo, and alternatively southward and northward at Millstone Hill. The net effect of plasma drifts at Arecibo, driven by the westward electric field (resulting in southward/downward $V_{\perp N}$) and southward wind (resulting in southward/upward $V_{\parallel}$, was basically in the horizontal direction during this interval. The plasma drifts at Millstone Hill experienced shorter-duration fluctuations. The decrease of electron density at both sites during the interval may be mostly attributed to chemical loss mechanisms, in spite of the plasma drift effects.

3.5. Diffuse Aurora and SAR Arc

During 0000-1000 UT on October 28 the all-sky imager operated at Millstone Hill. Figure 7 shows sample images of the 6300 Å emission. The bright feature to the north of Millstone Hill (top of the images) before ~0300 UT corresponds to the diffuse aurora as seen in many of our previous observations [e.g., *Mendillo et al.*, 1987, 1989; *Foster et al.*, 1994]. A faint SAR arc feature occurred to the north of the observing site after that time and stayed there for a few hours. Both the diffuse aurora and the SAR arc became brighter after ~0700 UT; the SAR arc then moved southward passing through zenith at Millstone Hill, shortly after ~0800 UT (~0300 LT).

A 6300 Å SAR arc is normally associated with the plasmapause region and related to the ionospheric heating process along magnetic field lines. The heating process arises from heat conduction between hot electrons coming from the magnetospheric ring current/plasmapause region and cold ionospheric electrons [e.g., *Rees and Roble*, 1975; *Kozyra et al.*, 1997]. The SAR arc usually occurs during the recovery phase of magnetic storms. As shown by the *Dst* results in Figure 2, this is indeed the case. The enhanced electron temperatures that cause the SAR arc were observed using the IS radar at Millstone Hill (Plate 2). Notice from Plate 2 that while the ion temperature did not change much, the electron temperature showed a pronounced maximum that shifted to lower latitudes during 0000-1000 UT on October 28. The motion of this high temperature region is clearly related to the equatorward motion of the SAR arc (Figure 7). We take this feature to mark the location of the plasmapause, and thus the magnetospheric shielding layer, in subsequent discussions.

4. Discussions

4.1. Ionospheric Dynamics at Millstone Hill

As presented in the previous sections, the daytime (October 27) zonal electric field perturbations at Millstone Hill seem to follow the enhancement and subsidence of both auroral electrojet and electric field at the high latitudes. The

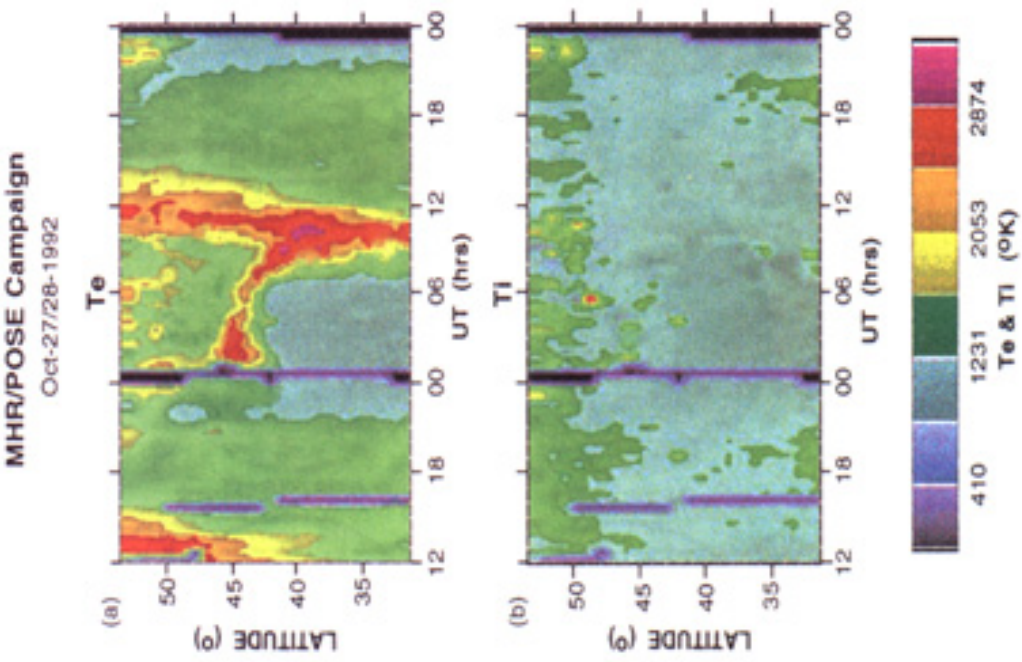

Plate 2. (a) Electron and (b) ion temperatures at 350 km measured using the Millstone Hill ISR during the POSE campaign. Data gaps in the ISR observations account for the features seen at 1600 UT (October 27) and 0000-0100 UT (October 28). The south-to-north T_e enhancements near 1000 UT mark sunrise effects. The high T_e zone for 0000-1000 UT marks the position of the trough/SAR arc at the plasmapause.

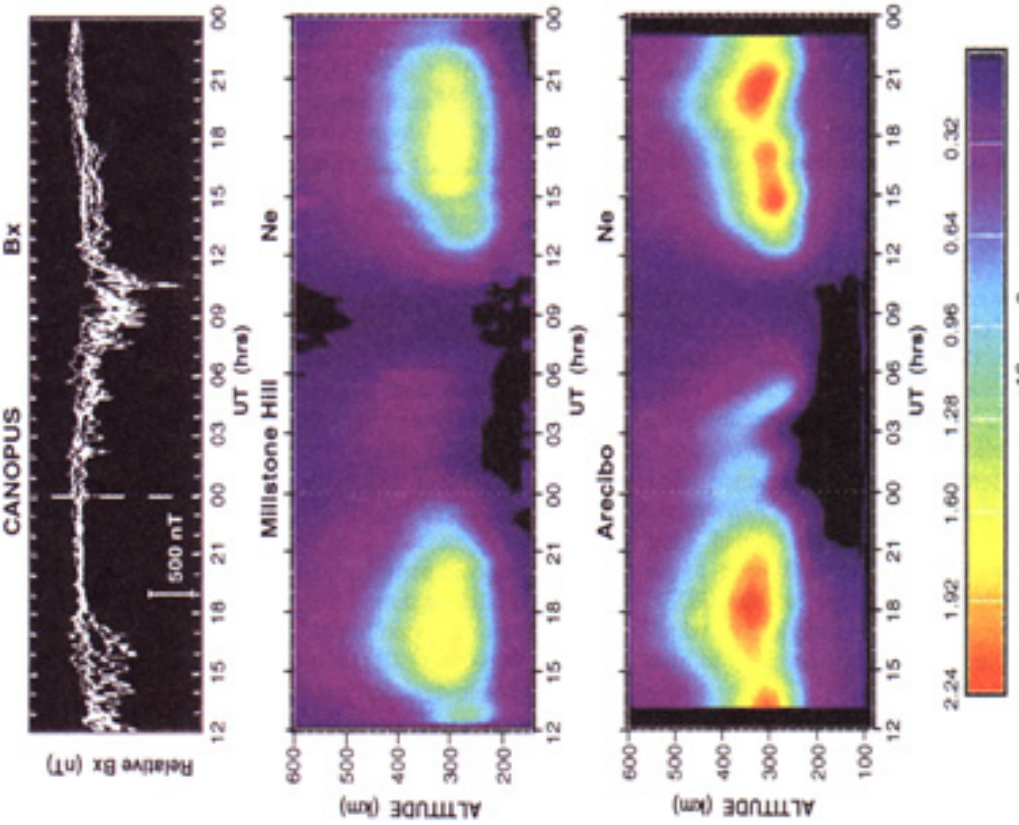

Plate 1. Plotted in contour (coded in color) are ionospheric electron densities measured by the incoherent scatter radars at Millstone Hill and Arecibo during October 27-28, 1992. The auroral electrojet *AU* and *AL* indices in the same period are also shown in the top panel to give the context of substorm activity.

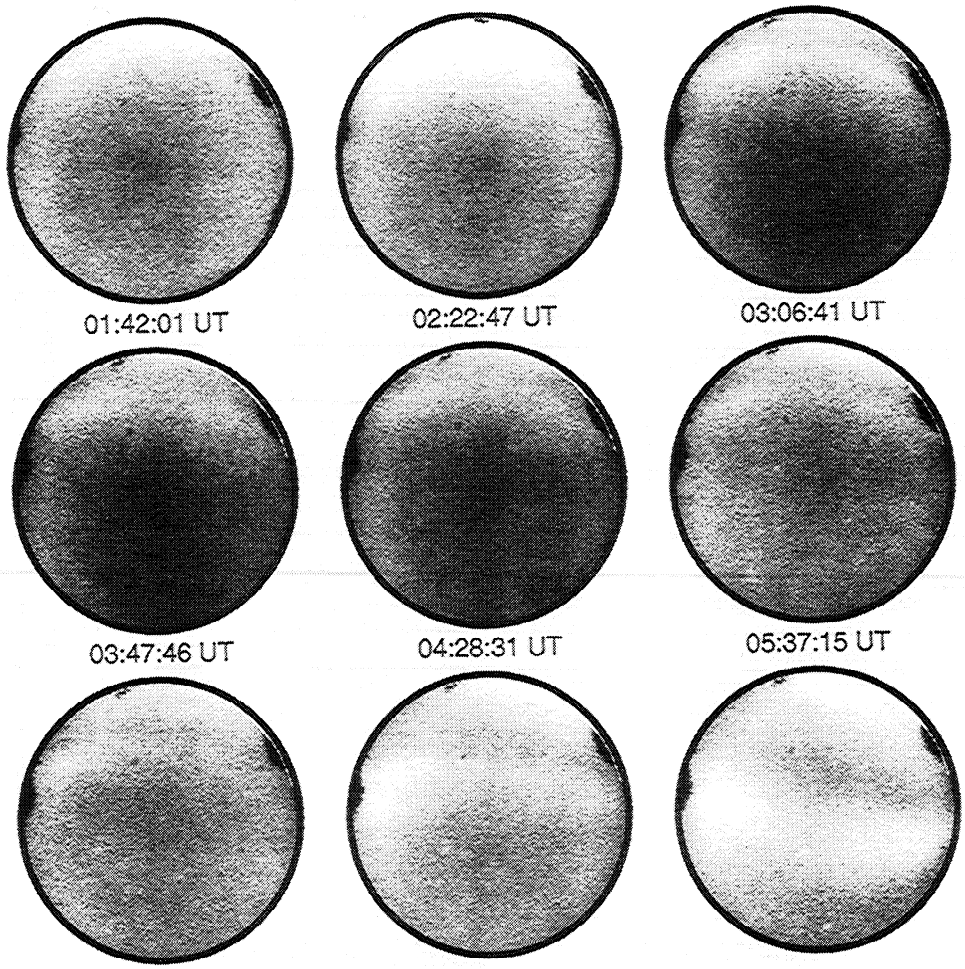

Figure 7. Images of 6300 Å emissions recorded by the CEDAR/BU Class-I Imager at Millstone Hill on October 28, 1992. The north is on the top, the east is on the left of each image, and the Millstone Hill observing site is at the center. The bright features in the far north of Millstone Hill appearing at 0142, 0223, and after 0537 UT are the diffuse aurora. An evident arc below the diffuse aurora is the SAR arc that moves southward starting at ~0730 UT.

pattern of alternating eastward and westward perturbations shows the characteristics of daytime electric field penetration and overshielding effects that have been suggested in previous studies [e.g., *Kelley et al.*, 1979; *Spiro et al.*, 1988; *Fejer et al.*, 1990; *Pi et al.*, 1993]. Other sources, however, are also able to drive middle-latitude electric fields during magnetic storms and substorms, such as disturbance wind dynamo effects [e.g., *Blanc and Richmond*, 1980; *Fejer et al.*, 1983]. To examine the wind dynamo effects, global wind circulation changes or global current systems need to be investigated. This was beyond the scope of the POSE campaign. However, comparisons between meridional winds and zonal electric fields at individual sites may help to give some hint about the dynamo effects.

Figure 8 gives the meridional winds, obtained using both the radar and FPI techniques, and the plasma $V_{\perp N}$ drift at Millstone Hill during the campaign. During the daytime event on October 27 at 1800 UT the plasma started drifting southward, and the wind remained northward but reduced its speed. The wind then changed its orientation ~1 hour later, with its speed staying smaller than $V_{\perp N}$ for ~3 hours. The fact that the wind tracked the plasma drift with a delay and with smaller speeds implies that ion drag might have caused neutrals to move in the same direction during this event. One needs to keep in mind that the standard ISR methods of deriving winds and perpendicular plasma drifts rely on several assumptions, such as no gradient in neutral winds. Nevertheless, the observations and the techniques described here are consistent with prior results [*Buonsanto and Foster*, 1993] that studied the effect of ion drag on winds at middle latitudes.

The observed perturbations of electric field and wind were more complicated during the nighttime event on October 28. First, when the meridional wind was strongly southward during 0000-0500 UT (1900-0000 LT), the plasma drift was in the opposite direction starting from 0200 UT. There are no clear indicators of a relationship between the wind and $V_{\perp N}$ during this period. This leads to a suggestion that the eastward electric field perturbation (the driver of northward $V_{\perp N}$) during this interval may come from magnetospheric electric field penetration, recalling that there was an eastward electric field surge at Sondre Stromfjord during the time (Figure 4). During 0500-0900 UT (0000-0500 LT), when the auroral electrojet was enhanced, the Millstone Hill radar data

showed opposite phase oscillations in $V_{\perp N}$ and neutral wind. After 0900 UT the wind and $V_{\perp N}$ seem to follow one another, indicating horizontal motions and coupling between neutrals and ions. The southward ($V_{\perp N}$) at Millstone Hill, however, seemed to follow the subsidence of zonal electric field perturbations at the Sondre Stromfjord (recalling Figure 5) 0600-0800 UT (0230-0430 LT for the site). These suggest that a possible overshielding effect was superimposed by the penetration of magnetospheric electric field as substorm activity was newly enhanced. Besides, the westward electric field at Millstone Hill also contributed to the equatorward motion of the SAR arc observed at the same site during 0700-1000 UT.

The equatorward motion of the SAR arc implies plasmaspheric compression on the night of the campaign. Similar dynamical features have been reported in satellite observations of H^+ and a SAR arc [*Chappell et al.*, 1971]. It was shown that under disturbed magnetic conditions the SAR arc location closely followed the position of the plasmapause to latitudes of L=2.5 or lower in the postmidnight sector. In the POSE campaign the southward motions of the hot electron region and SAR arc coincided with the westward electric field. These characteristics support the idea that plasmasphere compression, or inward convection of the plasmaspheric flux tubes, is associated with other magnetospheric processes causing the dynamical behavior of the SAR arc. One important consequence of this scenario is that the electric field at Millstone Hill would become the unshielded magnetospheric electric field as the shielding layer moves to the south of Millstone Hill.

4.2. Interplays between Electric Field and Meridional Wind at Arecibo

At Arecibo the plasma perpendicular drift ($V_{\perp N}$) perturbation during the postmidnight period (0600-0830 UT on October 28) shows a correspondence between the westward electric field perturbation and the enhancement of substorm activity. This seems to be consistent with the basic penetration characteristics. $V_{\perp N}$ at this site did not follow the shorter-duration (~0.5-1 hour) perturbations occurring at the higher latitudes, which might be due to the lower resolution of the data at this site. In order to examine possible wind-driven dynamo effects the ISR data at Arecibo were plotted in Figure 9 for further comparisons between the winds and the electric fields.

As shown in Figure 9, there existed an anticorrelation between $V_{\perp N}$ and $V_{\parallel}$ during 0300-1800 UT on October 28 at Arecibo, i.e., when $V_{\perp N}$ was in the downward/southward direction, $V_{\perp N}$ was upward/southward. The anticorrelation between the drifts at Arecibo has been studied in some previous works, and the phenomenon was attributed to the interplays between ions and neutrals or between electric fields and neutral winds at this latitude (the dip angle I=47°) [e.g., *Behnke and Harper*, 1973; *Rishbeth et al.*, 1978; *Oliver et al.*, 1988; *Buonsanto and Foster*, 1993]. In those works, suggestions were made to determine cause-effect mechanisms of electric fields and winds, such as comparing the strength and the timing between the two players. When neutrals drive ions, the anticorrelated motions of $V_{\parallel}$ and $V_{\perp N}$ should start at the same time, and the horizontal ion drift should be smaller than the horizontal neutral wind. On the other hand, when the electric field dominates, a wind may be induced via the ion-drag effect, and the wind speed should be smaller than the horizontal ion drift. In the latter scenario the wind should also follow the **E**×**B**-driven plasma drifts in the horizontal direction with a time delay, because it takes some time for ions to set much denser neutrals into motion. The time constant for such an effect varies due to daily variations of electron density, and can be estimated via

$$\delta t = (2\times10^{15}/N_e)(\delta u B/E) \qquad \text{s},$$

where δu is the velocity change of neutrals [*Kelley*, 1989]. For a density of 4×10^{11} m^{-3} (N_m at 0700 UT, October 28), it takes ~1.4 hours to accelerate neutrals to a velocity u comparable to E/B. As N_e becomes smaller, the effect is weaker and the longer time is required. As shown in Figure 9c, the plasma horizontal drift component V_{ph}, caused by $V_{\perp N}$, turned to southward at ~0630 UT, which was against the neutral wind horizontally. About 2 hours later the wind also turned to the southward direction, and its speed was smaller than V_h most of the time before 1030 UT, where V_h is the plasma total horizontal drift caused by both $V_{\perp N}$ and $V_{\parallel}$. These observations suggest that the driving force during 0630-1030 UT included the external electric field related to the magnetospheric substorm activity. Hence interpretation of the case presented here is that the southward plasma drift, driven by a possible overshielding effect, played a role of inducing a southward wind via the ion drag, which in turn contributed to the upward field-aligned plasma motion. However, this does not exclude the possibility of a southward wind surge due to the Joule heating effect in the auroral zone.

In contrast to the interval of 0630-1030 UT on October 28, interplay between the electric field and the neutral wind at Arecibo was reversed during 0330-0630 UT and 1200-1800 UT on the same day. In these intervals the wind speeds were greater than V_h most time and the anticorrelated plasma drifts started at the same times. This suggests that the plasma perpendicular drifts at these times were induced by the wind-driven dynamo effect.

4.3. Ionospheric Responses

As already presented in detail in the previous sections, dynamical effects caused ionospheric TEC changes at middle latitudes during the day of October 27, driven either by the meridional wind or the zonal electric field. This supports our previous modeling results in which the daytime TEC increase or decrease is attributed to the plasma life time changes as the plasma moves into different loss regions [*Pi et al.*, 1993, 1995]. The observations also indicate that the h_mF_2 rise or drop is positively correlated with both TEC and N_mF_2 variations during the daytime. Such correlations, however, do not apply at postmidnight times. In the absence of production, chemical loss mechanisms dominate in the determination of both TEC and N_mF_2 values, particularly at times close to the dawn. Greater chemical loss on the bottomside causes an apparent h_mF_2 increase even though the plasma drift mainly moves horizontally, as observed during the campaign. In addition, the very low level of electron densities, resulting from the dominance of chemical loss mechanisms, makes nighttime ionospheric responses to substorms, including TEC, N_mF_2, and h_mF_2, much less obvious on an absolute basis, as seen during 0700-1100 UT (0200-0600 LT) on October 28.

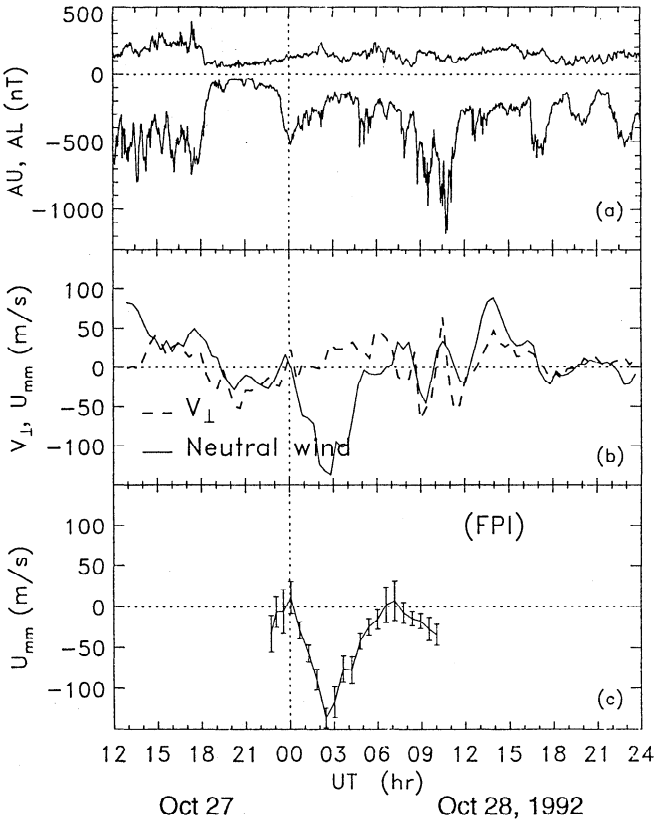

Figure 8. (a) The auroral electrojet *AU* and *AL* indices during October 27-28, 1992; (b) plasma $V_{\perp N}$ drift and meridional wind (positive northward) obtained using the Millstone Hill ISR; and (c) the meridional wind measured using an FPI at Millstone Hill.

5. Summary and Conclusions

An observational campaign focusing on ionospheric dynamics was conducted at Sondre Stromfjord, Millstone Hill, and Arecibo, spanning high, subauroral, and middle latitudes, on October 27-28, 1992. The observational techniques involved state-of-the-art ISRs, an all-sky CCD imager, an FPI, and magnetometers. During the 36-hour campaign, two periods of major substorm activity were recorded by the CANOPUS magnetometers, the first during the daytime on October 27 and the second during the nighttime on October 27-28.

The analyses presented in this paper show that the complexity of substorm effects upon the ionosphere-thermosphere becomes more obvious the greater the number of sites and diagnostics used. To try to synthesize the observational effects presented, we offer Figure 10 as an attempt to summarize processes acting during each phase of the disturbed periods (Figure 10a) within the context of an overall geomagnetic storm (Figure 10b) that occurred.

In Figure 10c the Sondre Stromfjord radar was used to monitor magnetospheric electrodynamical input. Under substorm conditions the observed zonal electric field at this high latitude site was eastward at noontime and westward (with eastward perturbations) at nighttime. In both instances these zonal electric fields were enhanced to ~60-80 mV/m eastward when major substorm activity (δB_x ~ 500-800 nT) occurred. For the meridional electric field, northward perturbations occurred during the daytime event, while at night it was southward with northward fluctuations when the auroral electrojets were enhanced.

In Figure 10d and 10e, the daytime disturbances penetrated to Millstone Hill, but not to Arecibo; subsequently, Millstone Hill showed a classic overshielding effect. This pattern reinforces the standard model for the absence (or only temporary presence) of magnetospheric fields at midlatitude ionospheric heights during daytime substorm events. The nighttime event, however, was far less compatible with this picture. The onset and expansion of substorm activity spanned the dusk to midnight period (0000-1200 UT on October 28) with peak electrodynamic effects at midlatitudes found during the postmidnight hours (0600-1200 UT). From 0000 to 0500 UT, penetration of meridional fields occurred. Zonal fields at the middle latitudes showed mixed patterns of shielding, penetration, and overshielding during 0000-1200 UT. We suggest that these perturbations can hardly be separated from the fact that they fell within a period of a larger-scale geomagnetic storm with a well-formed ring current pattern that complicates the notion of a simple shielding layer between the ionosphere and the magnetosphere.

In Figure 10f, thermospheric winds at Millstone Hill and Arecibo show effects related to auroral forcing. For the daytime event the southward wind perturbations are attributed to ion drag effects initiated by the electrodynamic input. For

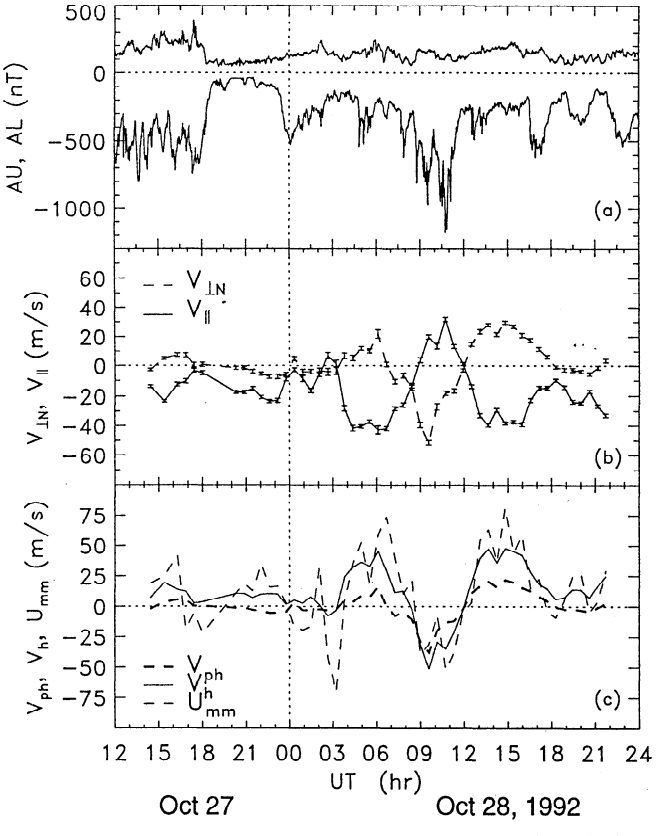

Figure 9. (a) The auroral electrojet *AU* and *AL* indices during October 27-28, 1992; (b) plasma drifts $V_{\perp N}$ (positive northward) and $V_\parallel$ (positive upward) obtained using the Arecibo ISR. In panel (c), the plasma total horizontal speed V_h, caused by both $V_{\perp N}$ and $V_\parallel$, and its component V_{ph}, caused by $V_{\perp N}$ only, are also compared with the meridional wind (U_{mm}) (positive northward) obtained using the ISR technique at the same site.

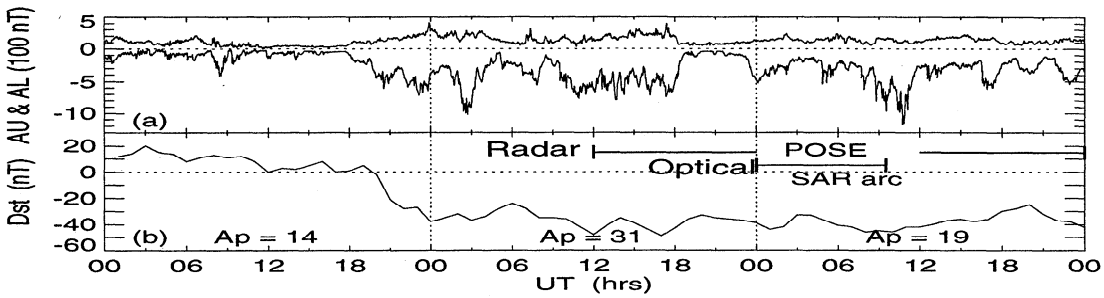

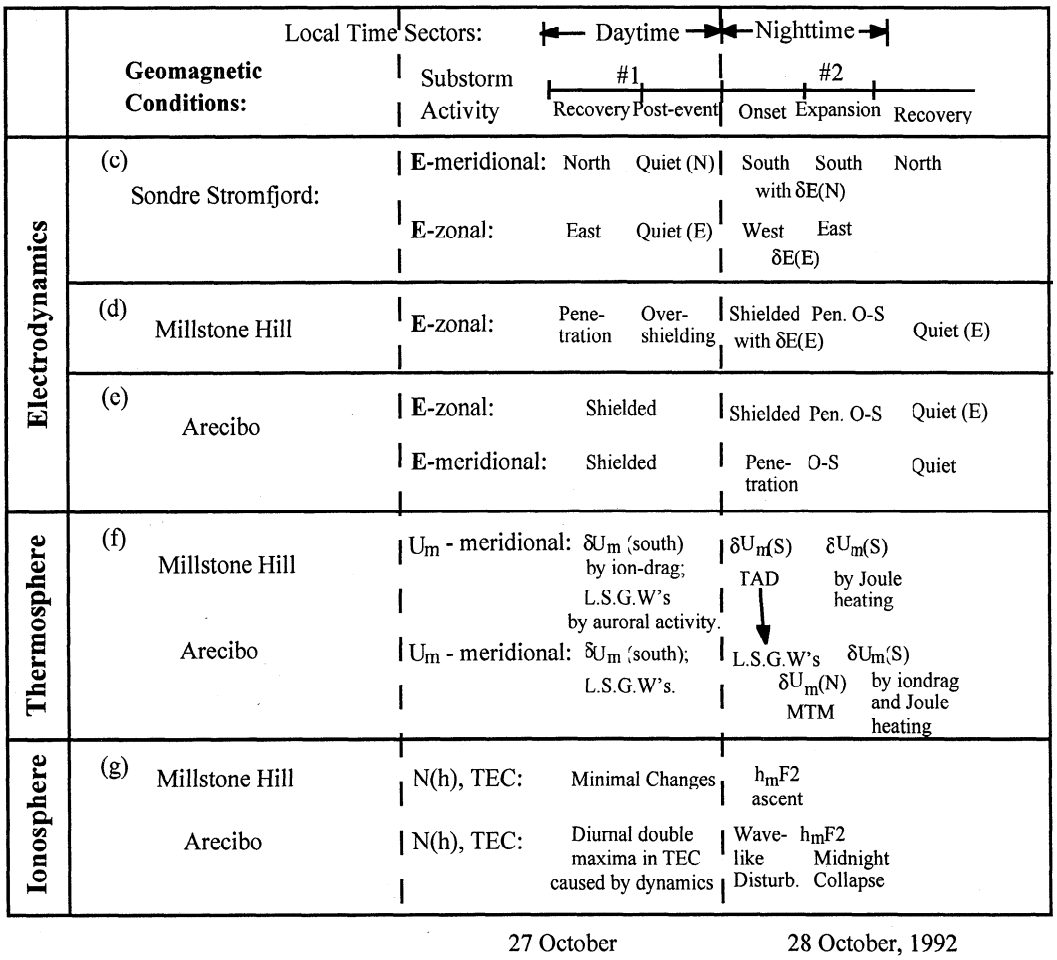

Figure 10. A synthesis of the dominant results of the POSE campaign, as presented in previous figures. (top) Geomagnetic indices and local time context information; (c-e) the electric field patterns at Sondre Stromfjord are related to Millstone Hill and Arecibo pattens as either penetration (pen), shielding, or over-shielding (O-S) events. (f) Neutral winds are portrayed in meridional winds (U_m), perturbations in winds (δU_m) with north (N) or south (S) noted, and by large-scale-gravity waves (LSGW) or traveling atmospheric disturbances (TADs). (g) Ionospheric profiles, $N(h)$, total electron content (TEC), and height of peak density (h_mF_2) are described.

the nighttime event the equatorward surge at ~0230 UT is attributed to a traveling atmospheric disturbance (TAD) launched by auroral energy input; the TAD reaches Arecibo about an hour later. The subsequent northward wind perturbations at Arecibo may be driven by the following two processes: (1) a TAD from the southern hemisphere propagated past Arecibo or (2) a midnight pressure bulge, due to an enhanced midnight temperature maximum (MTM), caused a midnight surge in the northward winds (see *Mendillo et al.* [1997] for a recent discussion of these effects at Arecibo). Southern hemisphere winds (unavailable during POSE) would be required to sort out the reality of an interhemispheric TAD versus a normal or enhanced MTM induced collapse. Whatever the source of these winds, they induce plasma drift events at Arecibo via well-observed dynamo action, accounting for the seemingly contradictory dynamics of magnetospheric origin prior to ~0830 UT. The subsequent southward wind at Arecibo involved plasma drag driven by a possible overshielding effect that started acting ~2 hours earlier, in addition to a possible southward wind surge due to the Joule heating effect in the auroral zone.

The ionospheric F region profile changes found during the POSE campaign include several coupling effects between the thermosphere and ionosphere. In Figure 10g these are shown to include a TEC diurnal double maximum (DDM) at Arecibo during the daytime event. Its absence at Millstone is

suggestive of a thermospheric wind source since the dip angle at Arecibo is more favorable for wind-induced effects. Large-scale gravity waves (LSGWs) appear at both sites, probably caused by auroral heating effects. A wave-like disturbance during the evening on October 27 at Arecibo is identified in TEC, N_mF_2, h_mF_2, and electron density profiles, which is clearly due to a gravity wave shown in the meridional wind behavior. This gravity wave, with a period ~2.5 hours, is likely due to a TAD launched from the auroral zone. During the nighttime event, equatorward winds elevated h_mF_2 values which, in the absence of production, lead to a reduction in the normal decay rates, producing the ledges in h_mF_2 and TEC seen at both sites. This minimal decay period is terminated abruptly by a subsequent northward wind driven by either a TAD event from the other hemisphere or, more likely, an enhanced midnight pressure bulge effect. While geomagnetically induced changes in MTM effects (driven by semidiurnal tidal processes, as modeled by *Fesen* [1996] is a topic not yet explored by simulation work, evidence for enhanced MTM effects and particularly large midnight collapse events haven been seen at Arecibo during disturbances [*Mendillo et al.*, 1997].

Acknowledgments. The authors thank John C. Foster and John M. Holt at Haystack Observatory, MIT, and MaryMcCready at SRI International for their help in the POSE campaign. The Arecibo Observatory is part of the National Astronomy and Ionospheric Center, operated by Cornell University under a cooperative agreement with the NSF. The CANOPUS instrument array was constructed and is maintained and operated by the Canadian Space Agency. The work conducted at Boston University was supported, in part, by the NSF under grants ATM-9402269 and ATM-9612938.

Janet G. Luhmann thanks Gerd W. Prölss and another referee for their assistance in evaluating this paper.

References

Anderson, D. N., D. T. Decker, and C. E. Valladares, Modeling boundary blobs using time varying convection, *Geophys. Res. Lett., 23*, 579, 1996.

Anderson, D. N., *et al.*, Intercomparison of physical models and observations of the ionosphere, *J. Geophys. Res., 103*, 2179, 1998.

Bailey, G. J., R. Sellek, and Y. Rippeth, A modelling study of the equatorial topside ionosphere, *Ann. Geophys., 11*, 263, 1993.

Baumgardner, J., and S. Karandanis, CCD system using video graphics controller, *Electron. Imag., 3*, 28, 1984.

Baumgardner, J., M. Mendillo, and B. Flynn, Monochromatic imaging instrumentation for applications in aeronomy of the earth and planets, *Opt. Eng., 32*(12), 3028, 1993.

Behnke, R. A., and R. M. Harper, Vector measurements of*F* region ion transport at Arecibo, *J. Geophys. Res., 78*, 8222, 1973.

Biondi, M. A., J. W. Meriwether Jr., B. G. Fejer, S. A., Gonzalez, and D. C. Hallenbeck, Equatorial thermospheric wind changes during the solar cycle: Measurements at theArequipa, Peru, from 1983 to 1990, *J. Geophys. Res., 96*, 15,917, 1991.

Blanc, M., and A. D. Richmond, The ionospheric disturbance dynamo, *J. Geophys. Res., 85*, 1669, 1980.

Buonsanto, M. J., A case study of the ionospheric storm dusk effect, J. *Geophys. Res., 100*, 23,857, 1995.

Buonsanto, M. J., and J. C. Foster, Effects of magnetospheric electric fields and neutral winds on the low-middle latitude ionosphere during the March 20-21, 1990, storm, *J. Geophys. Res., 98*, 19,133, 1993.

Buonsanto, M. J., and J. M. Holt, Measurements of gradients in ionospheric parameters with a new nine position experiment at Millstone Hill, *J. Atmos. Terr. Phys., 57*, 705, 1995.

Buonsanto, M. J., J. C. Foster, A. D. Galasso, D. P. Sipler, and J. M. Holt, Neutral winds and thermosphere/ionosphere coupling and energetics during the geomagnetic disturbances of March 6-10, 1989, *J. Geophys. Res., 95*, 21,033, 1990.

Buonsanto, M. J., M. E. Hagan, J. E. Salah, and B. G. Fejer, Solar cycle and seasonal variations in *F* region electrodynamics at Millstone Hill, *J. Geophys. Res., 98*, 15,677, 1993.

Burns, A. G., T. L. Killeen, G. R. Carignan, and R. G. Roble, Large enhancements in the O/N_2 ratio in the evening sector of the winter hemisphere during geomagnetic storms, *J. Geophys. Res., 100*, 14,661, 1995.

Burnside, R. G., R. A. Behnke, and J. C. G. Walker, Meridional neutral winds in the thermosphere at Arecibo: Simultaneous incoherent scatter and Airglow observations, *J. Geophys. Res., 88*, 3181, 1983.

Burnside, R. G., J. C. G. Walker, and M. P. Sulzer, Kinematic properties of the *F* region ion velocity field inferred from incoherent scatter radar measurements at Arecibo, *J. Geophys. Res., 92*, 3345, 1987.

Chappell, C. R., K. K. Harris, and G. W. Sharp, Ogo 5 measurements of the plasmasphere during observations of stable auroral red arcs, *J. Geophys. Res., 76*, 2357, 1971.

Fejer, B. G., The electrodynamics of the low-latitude ionosphere: Recent results and future challenges, *J. Atmos. Sol.Terr. Phys. 59*, 1465, 1997.

Fejer, B. G., *F* region plasma drifts over Arecibo: Solar cycle, seasonal, and magnetic activity effects, *J. Geophys. Res., 98*, 13,645, 1993.

Fejer, B. G., et al., Low- and mid-latitude ionospheric electric fields during the January 1984 GISMOS campaign, *J. Geophys. Res., 95*, 2367, 1990.

Fejer, B. G., M. F. Larsen, and D. T. Farley, Equatorial disturbance dynamo electric fields, *Geophys. Res. Lett., 10*, 537, 1983.

Fesen, C. G., Simulations of the low-latitude midnight temperature maximum, *J. Geophys. Res., 101*, 26,863, 1996.

Foster, J. C., M. J. Buonsanto, M. Mendillo, D. Nottingham, F. J. Rich, and W. Denig, Coordinated stable auroral red arc observations: relationship to plasma convection, *J. Geophys. Res., 99*, 11,429, 1994.

Fuller-Rowell, T.J., M. V. Codrescu, E. Araujo-Pradere, and I. Kutiev, Progress in developing a storm-time ionospheric correction model, *Adv. Space Res., 22(6)*, 821-827, 1998.

Fuller-Rowell, T. J., M. V. Codrescu, R. J. Moffett, and S. Quegan, Response of the thermosphere and ionosphere to geomagnetic storms, *J. Geophys. Res., 99*, 3893, 1994.

Hedin, A. E., MSIS-86 thermospheric model, *J. Geophys. Res., 92*, 4649, 1987.

Hedin, A. E., *et al.*, Revised global model of thermosphere winds using satellite and ground-based observations, *J. Geophys. Res., 96*, 7657, 1991.

Kelley, M. C., *The Earth's ionosphere*, Academic, San Diego, Calif., 1989.

Kelley, M. C., B. G. Fejer, and C. A. Gonzales, An explanation for anomalous ionospheric electric fields associated with a northward turning of the interplanetary magnetic field, *Geophys. Res. Lett., 6*, 301, 1979.

Kozyra, J. U., Nagy, A. F., and D. W. Slater, High-altitude energy source(s) for stable auroral arcs, *Rev. Geophys., 35*, 155, 1997.

Lu, G., X. Pi, A. D. Richmond, and R. G. Roble, Variations of total electron content during geomagnetic disturbances: A model/observation comparison, *Geophys. Res. Lett.*, 15, 253, 1998.

Mendillo, M., J. Baumgardner, J. Aarons, J. Foster, and J.Klobuchar, Coordinated optical and radio studies of ionospheric disturbances: Initial results from Millstone Hill, *Ann. Geophys., 5A*, 543, 1987.

Mendillo, M., J. Baumgardner, and J. Providaker, Ground-based imaging of detached arcs, ripples, in the diffuse aurora, and patches of 6300 Å emission, *J. Geophys. Res., 94*, , 5367, 1989.

Mendillo, M., X. Q. He, and H. Rishbeth, How the effects of winds and electric fields in F_2-layer storms vary with latitude and longitude: A theoretical study, *Planet. Space Sci., 40*, 595, 1992.

Mendillo, M., J. Baumgardner, D. Nottingham, J. Aarons, B. Reinisch, J. Scali, and M. C. Kelley, Investigations of thermospheric ionospheric dynamics with 6300-angstrom images from the arecibo observatory, *J. Geophys. Res., 102*, 7331, 1997.

Oliver, W. L., S. Fukao, T. Sato, T. Tsuda, S. Kato, I. Kimura, A. Ito, T. Saryo, and T. Araki, Ionospheric incoherent scatter measurements with the MU radar: Observations of *F* region electrodynamics, *J. Geomagn. Geoelectr., 40*, 963, 1988.

Pi, X., M. Mendillo, M. W. Fox, and D. N. Anderson, Diurnal double maxima patterns in *F* region ionosphere: Substorm-related aspects, *J. Geophys. Res., 98*, 13,677, 1993.

Pi, X., M. Mendillo, P. Spalla, and D. N. Anderson, Longitudinal effects of the ionospheric responses to substorms at middle and lower latitudes: A case study, *Ann. Geophys., 13*, 863, 1995.

Prölss, G. W., Magnetic storm associated perturbations of the upper atmosphere: Recent results obtained by satellite-borne gass analyzers, *Rev. Geophys., 18*, 183, 1980.

Prölss, G. W., *Ionospheric F Region Storms, Handbook of Atmospheric Electrodynamics,* vol. 2, pp. 195-248, edited by H. Volland, CRC Press, Boca Raton, Fla., 1995.

Reddy, C. A., S. Fukao, T. Takami, M. Yamamoto, T. Tsuda, T. Nakamura, and S Kato, A MU radar-based study of mid-latitude *F*-region response to a geomagnetic disturbance, *J. Geophys. Res., 95*, 21,077, 1990.

Rees, M. H., and R. G. Roble, Observations and theory of the formation of stable auroral red arcs, *Rev. Geophys., 13*, 201, 1975.

Richards, P. G., and P. J. Wilkinson, The ionosphere and thermosphere at southern midlatitudes during the November 1993 ionospheric storm: A comparison of measurement and modeling, *J. Geophys. Res., 103*, 9373, 1998.

Richmond, A. D., E. C. Ridley, and R. G. Roble, A thermosphere/ionosphere general circulation model with coupled electrodynamics, *Geophy. Res. Lett., 19*, 601, 1992.

Rishbeth, H., *F*-region storms and thermospheric circulation, *J. Atmos. Terr. Phys., 37*, 1055, 1975.

Rishbeth, H., S. Ganguly, and J. C. G. Walker, Field-aligned and field-perpendicular velocities in the ionospheric F_2-layer, *J. Atmos. Terr. Phys., 40*, 767, 1978.

Roble, R. G., J. M. Forbes, and F. A. Marcos, Thermospheric dynamics during the March 22, 1979, magnetic storm, 1, Model simulations, *J. Geophys. Res., 92*, 6045, 1987.

Rostoker, G., J. C. Samson, F. Creutzberg, T. J. Hughes, D. R. McDiarmid, A. G. McNamara, A. Vallance Jones, D. D. Wallis, L. L. Cogger, CANOPUS - A ground based instrument array for remote sensing the high latitude ionosphere during the ISTP/GGS Program, *Space Sci. Rev., 75*, 743, 1995.

Schunk, R. W., and J. J. Sojka, A three-dimensional time-dependent model of the polar wind, *J. Geophy. Res., 94*, 8973, 1989.

Sipler, D. P., M. E. Hagan, M. E. Zipf, and M. A. Biondi, Combined optical and radar wind measurements in the *F* region over Millstone Hill, *J. Geophys. Res., 96*, 21,255, 1991.

Sojka, J. J., R. W. Schunk, M.D. Bowline, J. Chen, S. Slinker, and J. Fedder, Driving a physical ionospheric model with a magnetospheric MHD model, *J. Geophys. Res., 102*, 22209, 1997.

Spiro, R. W., R. A. Wolf, and B. G. Fejer, Penetration of high-latitude-electric-field effects to low latitudes during SUNDIAL 1984, *Ann. Geophys., 6*, 39, 1988.

Wickwar, V. B., J. W. Meriwether Jr., P. B. Hays, and A. F. Nagy, The meridional thermospheric neutral wind measured by radar and optical techniques in the auroral region, *J. Geophys. Res., 89*, 10,987, 1984.

M. J. Buonsanto and D. P. Sipler, Atmospheric Sciences Group, Haystack Observatory, MIT, Westford, MA, 01886. (dps@hyperion.haystack.edu.)

T. J. Hughes, Herzberg Institute of Astrophysics, NRC of Canada, 100 Sussex Drive, Ottawa, ON, Canada, K1A 0R6. (hughes@canott.dan.sp-agency.ca)

W. J. Hughes and M. Mendillo, Center for Space Physics, Boston University, 725 Commonwealth Ave, Boston, MA 02215; (mendillo@buasta.bu.edu)

J. D. Kelly. SRI International, 333 Ravenswood Ave, Menlo Park, CA 94025; (kelly@sri.com.)

G. Lu. High Altitude Observatory, NCAR, P.O.Box 3000, Boulder, CO 80307-3000. (ganglu@ncar.ucar.edu.)

X. Pi, Jet Propulsion Laboratory, California Institute of Technology, MS 138-308, 4800 Oak Grove Drive, Pasadena, CA 91109-8099. (Xiaoqing.Pi@jpl.nasa.gov.)

Q. Zhou, Arecibo Observatory, NAIC, Arecibo, Puerto Rico 00613-0995; (zhou@naic.edu.)

(Received June 16, 1998; revised October 13, 1999;
accepted October 13, 1999)